DRAFT SF 298

1. Report Date (dd-mm-yy)	2. Report Type	3. Dates covered (from... to)

4. Title & subtitle	5a. Contract or Grant #
Corrosion Consequences of Molten Salt Deposits in Combustion Turbines Burning Vanadium Contaminated Liquid Fuel Tri-Service Conference on Corrosion Proceedings	
	5b. Program Element #

6. Author(s)	5c. Project #
Rathnamma, Dasara V. Nagarajan, R.	5d. Task #
	5e. Work Unit #

7. Performing Organization Name & Address	8. Performing Organization Report #

9. Sponsoring/Monitoring Agency Name & Address	10. Monitor Acronym
Tri-Service Committee on Corrosion USAF WRIGHT-PATTERSON Air Force Base, Ohio 45433	
	11. Monitor Report #

12. Distribution/Availability Statement
Approved for Public Release
Distribution Unlimited

13. Supplementary Notes

14. Abstract

15. Subject Terms
Tri-Service Conference on Corrosion

Security Classification of			19. Limitation of Abstract	20. # of Pages	21. Responsible Person (Name and Telephone #)
16. Report	17. Abstract	18. This Page			

TRI-SERVICE CONFERENCE ON CORROSION

1994 TRI-SERVICE
DEPARTMENT OF DEFENSE
UNITED STATES OF AMERICA
CONFERENCE ON CORROSION

21-23 JUNE 1994

SHERATON PLAZA HOTEL
ORLANDO, FLORIDA

PROCEEDINGS

CORROSION CONSEQUENCES OF MOLTEN SALT DEPOSITS IN COMBUSTION TURBINES BURNING VANADIUM CONTAMINATED LIQUID FUEL

*Dasara V. Rathnamma
N~··al Surface Warfare Center,Carderock Division
code 642,3A Leggett Circle
Annapolis, MD 21402-5067

R. Nagarajan
IBM Corporation,5600 Cottle Road,San Jose, CA 95193-0001

ABSTRACT

Molten salts condensing on marine turbine blades can dissolve the protective oxide coating and catastrophically attack the exposed alloy surface beneath-- a process known as hot corrosion. We present here the implications of a theoretical model of hot corrosion rate that is limited by diffusional dissolution of oxide species into the melt for the design of burner-rigs to test the corrosion-resistance of superalloy materials. Parameters expected to govern the dissolution rate of a given oxide are the rate of deposition of the multicomponent(sulfate-vanadate-oxide)'solvent'-liquid,liquid-layerthickness,and composition-dependent physical properties of the deposit, such as density and viscosity. The solid portion of deposit mass, being relatively inert with respect to hot corrosion, will not correlate well with experimental corrosion rates. These hypotheses are tested by comparing our model-predictions with one set of burner-rig corrosion rate measurements made during the combustion of vanadium-containing liquid fuel seeded with the same concentration of various metallic additives. Our findings indicate that the total weight (solids + liquid) of the deposit has no direct correspondence with its corrosive potential. However, additives that are effective in suppressing liquid phase formation will, in general, reduce the corrosion rate equally effectively. Liquid mass arrival rate and oxide

solubility in the liquid are quantities of relevance to the problem, but the best correlation of experimental data with theory is obtained for the oxide dissolution rate (which is approximately inversely proportional to the liquid layer thickness). Thus, burner-rigs designed to simulate either of these two parameters will reproduce the hot-corrosion characteristics of the engine with reasonable accuracy.

1. INTRODUCTION

1.1 Molten Salt Deposition and Its Corrosion Consequences:

Nickel-base superalloys, used extensively for gas turbine (GT) engine components because of their superior high temperature mechanical properties, are susceptible to a form of environmental attack known as hot corrosion. Hot corrosion is encountered when molten salts, e.g., sodium sulfates and vanadates, are deposited (as pure liquids or in solution) from the product gases of combustion onto turbine blades and guide-vanes. The adverse effects of molten alkali salt condensation have paralleled the growth of high-temperature energy technologies. Among such technologies are: coal gasification, direct coal-fired turbines, magneto hydrodynamic(MHD), molten salt fuel cells and of primary interest here, marine engines operating on vanadium-contaminated liquid fuels.

Blade surfaces are usually coated with metal alloys that form an adherent, refractory and corrosion-resistant oxide-layer on the gas-side of the coating. The following mechanism has been proposed[1] for the initiation and propagation of hot corrosion: At locations where the protective oxide scale is partially leached or completely dissolved by the condensed molten salt-'solvent', the metal substrate is more accessible, hence vulnerable to catastrophic corrosion. Local saturation of the liquid layer is prevented by dynamic fluxing due to aerodynamic- and centrifugal-shear forces which convey dissolved oxide from the site of dissolution to the tip and trailing-edge regions of the blade. The oxide dissolution rate is taken to be limited by high-Schmidt number Brownian diffusion of the oxide species in the melt (as well as by salt/oxide interfacial detachment kinetics). Thus (composition-dependent) deposit physicochemical properties such as density, viscosity, oxide diffusivity and solubility, and thickness will influence the oxide dissolution rate. Other parameters that will play a role include aerodynamic variables such as the convective flux of the gas phase alkali contaminants,

<center>2</center>

and material integrity characteristics of the blade alloy surface.

1.2 Burner-Rig Testing: An Assessment of Hot Corrosion Simulation Criteria

At present no standard testing procedure exists for determining the hot corrosion resistance for alloys of construction.   Time and economy considerations have led to the development of two general types of laboratory hot salt corrosion test procedures, one involving burner rigs, the other involving furnaces. Comparison of the morphology of the corrosion product with that found on GT blades and other hot-section components indicates that burner-rig testing gives the most realistic simulation of service behavior[2]. However, even if dynamic testing under tightly-controlled condition were to be performed in burner rigs, the success of the simulation effort would necessarily be judged on the basis of acquired ability to interpret and properly extrapolate test results to the real engine. This classical 'scale-up' problem demands an understanding of the mechanism of hot corrosion. We need to know what initiates it, what sustains it, at what rate it proceeds, and how the rate is related to the rate of deposition of the corrosive liquid.

Given the abundance of key variables in this hot-corrosive environment, (cf. Section 1.1) it is not surprising that a review of simulation criteria reported in literature reveals a wide spectrum of views regarding the crucial parameter on which to base the design of the test-rig. It has been reported[3,4,5]. that hot corrosion (sulfidation) in gas turbines occurred only in places where alkali sulfates formed a molten deposit. Therefore, they suggest that the melting-point temperature, T_{mp}-- the 'threshold' temperature for initiation of the sulfidation attack-- and the dewpoint temperature, T_{dp}-- the 'terminal' temperature above which no sulfidation can occur-- be reproduced in the rig[6]. It has been studied that the chemical behavior of deposit forming components (sodium, vanadium, chlorine, sulfur) of GT flue gases, and concluded that the multicomponent salt physical chemistry needs to be reproduced in the low-pressure burner rig by appropriate elemental additions to the fuel. Studies[7] suggest on the basis of laboratory results that rig and engine tests should be compared in terms of the amount of contaminant passing through unit area in unit time. Studies advocate[8] that the partial pressure of the alkali vapor precursor be kept equal in the low- and high-pressure combustors. It has been identified[9] that deposition rate of alkali salt from the vapor phase as the single most important factor in determining corrosion rates.   The amount of total deposit which collects on the blade surface dictates the rate of corrosive attack[10]. It has been

3

pointed out[11] that the thickness of the salt deposit is a key variable, often overlooked in mechanistic studies, in determining the transport of oxidant from the gas phase to the corrosion site. Some researchers[12] have proposed salt-'fluxing' of the underlying oxide layer as the rate-limiting step in the corrosion process. Computed relative oxide dissolution rate profiles would then be closely linked to corrosion 'maps' obtained experimentally[4]. The implication here is that these dissolution rate characteristics would have to be reproduced in a well-designed test-rig.

Comparison of these different simulation strategies for the same burner-rig (Figure 1) shows that each would result in a unique set of operating conditions chosen for the burner-rig. For instance, in order to reproduce the contaminant flux-rate characteristics of a 10 atmosphere turbine in an atmospheric pressure burner-rig, the Mach number (Ma) of combustion gas flow would have to be increased by a factor of about 8 over its engine value, and by a factor of more than 10 to simulate the engine deposition/oxide dissolution rates; whereas, in order to obtain an equivalent thickness of condensed salt, the rig Mach number would actually have to be lower than the engine Mach number. Thus, the choice of operating conditions for the burner-rig depends on the sensitivity of the parameter to be simulated. However, no firm conclusions were drawn, which of these simulation-strategies would give the best results. In this paper, we carry the analysis further, and demonstrate that a rig designed on the basis of equivalent oxide-dissolution rate will best simulate the corrosion characteristics of an operational turbine engine. This is done by means of comparisons of predicted deposition-related quantities, such as the deposition rate, the liquid layer thickness and oxide dissolution rate, with experimental hot corrosion (metal weight loss) data obtained on a burner rig. The effect of introducing the same level of various fuel-additives on observed hot corrosion rates is found to correlate best with the corresponding effect on computed oxide dissolution rate.

2. EXPERIMENTAL PROCEDURE

Corrosion rate-data used here for illustrative purposes were obtained from tests conducted in a battery of small atmospheric pressure combustion test rigs at David Taylor Naval Ship Research and Development Center (NSRDC). The fuel used in this investigation conforms to Specification MIL-F-859A, Burner Fuel Oil, Navy Special Grade. A listing of the properties of

this fuel may be found in the report[13]. AISI 310 alloy was chosen as the test material due to its widespread use; it is composed of 0.25% C, 24-26% Cr, 19-22% Ni, 1.5% Si and the balance Fe. Metallic additives tested with respect to their corrosion-inhibition capability were mostly metal-organic compounds in the form of oil-soluble naphthenates. Tests were conducted for a duration of 100 hours, mostly at a metal temperature of 1600 F. Upon completion of the tests, the specimens were photographed, weighed, and prepared for further analysis by removing the deposits in a molten salt bath. Specimen corrosion was measured as the difference in weight before test and after cleaning. Deposit weight was the weight difference between the untested specimen and the specimen after test exposure.

Data on weight change rate of the specimens from tests using an atomic ratio of six atoms of metal additive to one atom of vanadium in the fuel are plotted in bar diagram form in Figure 2. The amount indicated below the base line represents the weight loss, before and after descaling. The amount above the line indicates deposition of material from the gas stream plus the weight gain attributable to oxidation of the base material. The calculated weight gain due to the oxides is represented by the shaded portions of the total deposit bars. Figure 2 shows that lanthanum, iron and antimony are the most beneficial additives from the standpoint of both deposition and corrosion. Other metals seemingly worthy of consideration include magnesium, calcium, silicon, sodium, and rare earths such as cerium and neodymium. These favorable test data were, however, not exploited fully owing to a lack of fundamental understanding of the interdependency between the deposition and corrosion processes. Since additives influence corrosion primarily by modifying the deposition characteristics of the system, this proved to be a major obstacle. We have recently[14] analyzed the use of fuel additives to minimize corrosion of GT blade material in the following series of steps: first, a free-energy minimization computer program was employed for an equilibrium-thermodynamic prediction of condensed (ideal) solution composition; relevant physico-chemical properties of the molten solution were then estimated based on predicted equilibrium composition; oxide solubility and dissolution rate were then calculated for this solution in contact with various solid oxides. In this work, we will attempt to verify the model for the rate-determining process-- i.e., oxide dissolution-- in hot corrosion by comparison with appropriate hot corrosion test data, and by a process of elimination of other feasible parameters.

3. THEORETICAL MODEL TO PREDICT OXIDE DISSOLUTION RATE

The present model of hot-corrosion controlled by diffusion-limited dissolution of oxide species into the molten salt layer has been described fully[15,12], and also discussed[14,16]. The Brownian high-Schmidt number diffusional flux of oxide into the liquid may be represented as a product of a mass transfer coefficient and a concentration gradient:

$$j'_{0,w} = K_m \cdot (\omega_{0,w} - \omega_{0,b}) \qquad (1)$$

where ω_0 is the oxide mass fraction at the melt/oxide interface (w) or in bulk liquid solution (b), and k_m, the convective diffusion mass transfer coefficient is estimated[17]. It incorporates liquid density and viscosity, oxide diffusivity in liquid, local liquid layer thickness, upstream and local vapor deposition rates, and the total shear force exerted on the flowing liquid layer by the adjacent gas layer and the turbomachinery. For the sake of simplicity, the dissolution rate is estimated here for a stagnation line configuration, which is representative of the leading edge (LE) of a turbine blade and of the burner-rig geometry. In this limit of negligible liquid streamline flow, the local liquid layer thickness is calculated to be its 'stator-value':

$$\delta_r = [2\mu/(\frac{\partial \tau_{w,g}}{\partial x})_{x \cdot 0} (\frac{-\dot{m}_w + j'_{0,w}}{\rho_l})]^{1/2} \qquad (2)$$

with the inclusion of the dissolved oxide contribution to the total liquid mass. Here, μ_l is the liquid viscosity, $(\partial \tau_{w,g}/\partial x)_{x=0}$ the shear stress gradient at the LE $-\dot{m}''$ the local deposition rate of total liquid, and ρ_l the liquid density.

Individual liquid constituent properties, e.g., viscosity, freezing point, etc., and their temperature and/or composition dependencies are extracted from available literature and phase diagrams[18,19], and used as the basis for approximating the properties of multicomponent ideal solutions of these as arithmetic (weighted) means. The effect of nonideality, neglected here, can be incorporated as correction factor that is related closely to the heat of mixing[20]

In the present theory, single species diffusional fluxes to the surface are taken to be by single vapor precursor (e.g., $Na_2SO_4(g)$) concentration

6

diffusion through a chemically frozen boundary layer. In the multicomponent case, individual constituents still deposit by single vapor species diffusion, but their molar fluxes are constrained to be in the same ratio as their steady-state mole fractions in the condensed phase. A more detailed discussion of these aspects, and other capabilities and limitations of the present theory is available elsewhere[21,22,1].

4. RESULTS AND DISCUSSION

The Complex Chemical Equilibrium Calculation (CEC) computer program, originally developed at NASA Lewis Research Center[23] and recently modified to include multiple ideal solutions in the condensed phase, predicts that for the vanadium-contaminated fuel under consideration, the likely condensed species are: $Na_2SO_4(1)$, $NaVO_3(1)$ and $V_2O_5(1)$, in varying fractions depending on the relative levels of sea-salt and vanadium ingested, and the local pressure and temperature. Thermodynamic calculations indicate that most metallic additives tend to enrich Na_2SO_4 in the liquid phase by preferentially forming gaseous and solid compounds with the vanadium present. All additives (except sodium) also tend to decrease the total fraction of condensed liquid in the product mixture, implying a corresponding reduction in the extent of liquid-'catalyzed' corrosion. This system was investigated (with no additives)[24] thermodynamically to determine the effects of varying turbine operating conditions on the limiting fuel impurity levels that will lead to condensation, and to compute the compositions and amounts of deposits for varying levels of sodium and vanadium. They also report that the species listed above comprise most of the condensate, with minimal amounts of higher order vanadates ($Na_4V_2O_7$, Na_3VO_4). They have treated $NaVO_3$ as $Na_2V_2O_6$ and assumed that the Na_2SO_4-$Na_2V_2O_6$ mixture can be treated as an ideal solution. While their thermochemical analysis, which is extended over a wide composition range, necessarily deals with ternary Na_2SO_4-$Na_2V_2O_6$-V_2O_5 solutions, at the vanadium concentrations we are interested in, a simplified binary analysis (Na_2SO_4-$Na_2V_2O_6$) is generally adequate. The treatment in literature[24] contains no vapor-phase transport calculations of deposition rates, and no references to the subsequent corrosion process. These are the issues we will specifically address in the remainder of this paper.

The oxide dissolution rate responds to liquid phase composition and total changes acting in concert. According to the present model, magnesium,

7

cadmium, cobalt, manganese, and nickel are the most effective suppressors of dissolution-limited hot corrosion, whereas cerium and aluminum are among the less effective. Added sodium and potassium enhance the corrosion rate. These trends are in excellent agreement with the experimental findings[13]; A more detailed comparison of theory and practice in this regard is in literature[18]. Our concern here rests more with the effect of additives on several deposition-related quantities, and on whether the predicted effect on the oxide dissolution rate systematically parallels the effect on observed corrosion rate.

Toward this end, we have attempted to correlate corrosion data collected[13] with measured total weight (solids + liquid) of the deposit, as well as with calculated quantities such as the weight of the liquid portion of the deposit, the 'ideal' solubility of the oxide species in the liquid, the phase fraction of condensed material in the combustion product gases, the total deposition rate of the liquid, the liquid layer thickness and the oxide dissolution rate. Figures 3 through 7 represent our efforts at correlating these potentially important parameters with the corrosion rate. In these figures, we plot the logarithm of the nondimensionalized corrosion rate with no additives as a function of various nondimensional parameters that were determined for no additives. The rate and weight data used here were obtained under the conditions reported in Figure 2 (metal-to-vanadium atomic ratio of 6, surface temperature of 1600 F). The metallic additives whose effects were considered here are titanium, tin, barium, strontium, zinc, sodium, indium, calcium, nickel, iron, manganese, cadmium, cerium, neodymium and lanthanum (at an atomic ratio of 3 to vanadium). CEC-predicted solution compositions and condensed phase fractions corresponding to these additives and a surface temperature of 1600 F are presented in Table 1. Deposition-related calculations that went into the construction of Figures 5 through 7 are based on these computed compositions. At this atomic level of added metal, the dominant species in solution for all additives except titanium and cerium are found to be $Na_2SO_4(1)$ and $Na_2V_2O_6(1)$; for those two metals, the primary solution components are $Na_2V_2O_6(1)$ and $V_2O_5(1)$. In the case of zinc, all liquid-phase component mole fractions are negligibly small, suggesting that the addition of zinc results in the enrichment of the condensed phase in the relatively benign (with respect to hot corrosion) solids.

From Figure 3, it is clear that there is no systematic relationship between corrosion rates and total deposit weights, possibly due to the fact that the

solid part of the deposit is inert with respect to corrosion. Indeed, any additive (e.g., zinc) that tends to increase the solids fraction in the deposit will prove to be an effective suppressant of hot corrosion, whereas trace impurities that result in the formation of low-melting eutectics (e.g., sodium, potassium, iron) invariably exacerbate the corrosion problem. Figure 4 is a log-log plot of the corrosion rate (nondimensionalized) versus condensed liquid mole fraction in the combustion gases (nondimensionalized against its no-additive value). Again, no direct correspondence is detected between these quantities, although one qualitative trend may be detected: in general, smaller condensed liquid inventories correspond to reduced corrosion rates. Thus, additives that suppress liquid phase formation via, e.g., homogeneous vapor ₋hase chemical reactions that 'trap' condensible elements in ∽∽seous compound⸱ can prove beneficial in mitigating hot corrosion. This possibility was explored in our previous work on the use of fuel additives[14] to combat corrosion.

From Figure 5, it may be inferred that the oxide 'solubility' (here taken to be the saturation mass fraction of the oxide in the melt estimated at the temperature of the melt/oxide interface) does not directly correlate with measured corrosion rates either, although it does play a significant role in determining the oxide dissolution flux into the bulk liquid. Equilibrium-thermodynamic phase diagram analyses often employed to characterize the hot corrosion process on the basis of equilibrium-solubility of oxide species into molten-salt solvents are thus not complete representations of the corrosion situation. Corrosion rates are expected to be limited by mass-transport rates of the interfacial oxide from the solid phase into the liquid, and perhaps also by the kinetics of this interfacial-detachment process. The calculations shown in Figures 6 and 7, based on Fickian- and Brownian-rates of diffusion (of vapor to the wall, and of oxide into liquid, respectively), are thus likely to be more relevant to the liquid-induced corrosion problem than the previous analyses.

Figure 6 indicates that the deposition rate is a useful quantity to keep track of, since it obviously has an influence on the observed rate of hot corrosion. However, the coupling between the two may not be as close as previously suspected. As with the condensed liquid phase fraction, while the extremes match-- i.e., the additive that results in minimum deposition also brings about a minimum in corrosion rate, and the maxima coincide as well-- no systematic, physically-meaningful relationship between these two quantities emerges from our investigation (given the limitations of presently

9

available data). In Figure 7, we present results of correlating the corrosion rate data with other calculable deposition-related parameters-- viz., the liquid deposit weight, the liquid layer thickness and the rate of oxide dissolution into the liquid. An examination of this semi-logarithmic plot leads to the following important observations:

   o The corrosion rate is inversely proportional to the liquid layer thickness.

   o The corrosion rate is (approximately) inversely proportional to the weight of the liquid portion of the deposit.

   o The corrosion rate varies approximately linearly with predicted oxide dissolution rate.

The first two observations are understandable in light of the third. If the corrosion rate is limited by oxide diffusion across the liquid layer, the dissolution velocity, hence corrosion rate, of the oxide into the liquid may be approximated to be (at steady-state):

$$j'_{0,w}/\rho_l \approx D_{0,l}/\delta_l \qquad (3)$$

(Where $D_{0,l}$ represents the oxide diffusivity in liquid.)

   Thus, a direct linear dependence of the corrosion rate on oxide dissolution rate implies an inverse dependence on the liquid layer thickness. Both these trends are clearly visible from a comparison of our predictions with measured laboratory burner-rig corrosion rates, lending credence to our proposed fundamental mechanism of hot corrosion initiation. While we are constantly on the lookout for other data with which to verify our claim that the diffusional process of oxide dissolving into the condensed salt-solvent limits the rate at which the subsequent corrosion process proceeds, we are necessarily restricted at present to using Schab's data[13] as 'testing-ground' for our hypothesis. Readers with knowledge or data that will reinforce (or contradict) our basic theoretical concepts are urged to communicate these to the authors, so that progress may be sustained toward developing an 'international-standard' rig-testing procedure.

5. CONCLUSIONS

Our approach to the prediction of corrosion rates based on oxide dissolution into the condensed liquid has been found to be reasonably successful in explaining the effect of varying levels of any fuel additive, as well as the relative effect of the same level of various additives, on observed hot corrosion rates due to fuel impurities. We thus have a predictive tool that may be used to assist in the process of designing low-pressure corrosion simulation rigs, and in devising additive/fuel cleaning techniques to minimize corrosion of hot section components in marine gas turbines.

A critical re-examination of several elements of preliminary mechanistic theory presented in this paper indicates the following points:

1. While the 'chemically frozen' model of gas-phase chemistry is one tractable kinetic 'asymptote', the other would be one in which the gas-phase is in local thermochemical equilibrium (LTCE) everywhere. Deposition rates (and accompanying dissolution rates) computed in these two extremes of homogeneous kinetics are likely to be quite different in the high-temperature, dissociative environment of a combustor. Efforts were underway[1] to obtain the two limits within which observed deposition rates and dewpoints may be expected to lie for a given system.

2. Our model of non-reactive dissolution of oxide species into the molten salt liquid is of limited validity. The role of solvent/oxide interfacial kinetics and solvent/gas interfacial processes (e.g., gas-phase supersaturations, effect of vapor pressures on condensed phase electrochemistry, etc.) must be accounted for in a progressively more realistic model.

By the application of approximately the same principles, a model for molten salt corrosion of ceramics was developed[25] for GT model fuels.

A more advanced theoretical hot corrosion predictive model was developed[26].

11

6. REFERENCES

1.   ROSNER, D. E. and NAGARAJAN, R., 'Vapor Deposition and Condensate Flow on Combustion Turbine Blades: Theoretical Model to Predict/Understand Some Corrosion Rate Consequences of Molten Alkali Sulfate Deposition in the Field or Laboratory', Int. J. Turbo Jet Engines (in press, 1987)

2.   SANTORO, G. J., 'Hot Corrosion of Four Superalloys: HA-188, S-57, IN-617, and TD-NiCrAl', Oxic. Metals, 13, 405 (1973)

3.   DeCRESCENTE, M. A. and BORNSTEIN, N. S., 'Formation and Reactivity Thermodynamics of Sodium Sulfate with Gas Turbine Alloys', Corrosion, 24, 127-133 (1968)

4.   FRYXELL, R. E. and BESSEN, I. I., 'Coating Life Assessment in Gas Turbines Operated for Ship Propulsion', in Proceedings of 1974 Gas Turbine Materials in the Marine Environment Conference (J. W. Fairbanks, I. Maschlin, eds.), 24-26 July 1974, Marine Maritime Academy, Castine, Maine; p 259-276

5.   RENTZ, W. A., WALTERS, J. J. and FREEMAN, JR., W. R., 'A Dynamic Hot-Corrosion Rig Testing Procedure', J. Materials, 4, 520-539 (1969)

6.   HALSTEAD, W. D., Calculations on the Effects of Pressure and Temperature on Gas Turbine Deposition', in Deposition and Corrosion in Gas Turbines (A. B. Hart and A. J. B. Cutler, eds.), J. Wiley, 1973; p 22-23

7.   HANCOCK, P., "Rig Testing to Study Environmental Effects on Hot Corrosion Mechanisms', in Proceedings of 4th Conference on Gas Turbine Materials in the Marine Environment, 26-28 June 1979, U. S. Naval Academy, Annapolis, MD; p 465-473

8.   TSCHINKEL, J. G., 'Formation of Sodium Sulfate in Gas Turbine Combustors', Corrosion, 28, 161-169 (1972)

9.   SAUNDERS, S. R. J. and NICHOLLS, J. R., 'Hot Salt Corrosion Test Procedures and Coating Evaluation', Thin Dolid Films, 119, 247-269 (1984)

10.   LEE, S. Y., DeCORSO, S. M. and YOUNG, W. E., 'Laboratory Procedures for Evaluating High-Temperature Corrosion Resistance of Gas Turbine Alloys', ASME Trans., Ser. A. J. Engrg. Power, 93, 313-320 (1971)

11.   SHORES, D. A., 'New Perspectives on Hot Corrosion Mechanisms', in High Temperature Corrosion (R. A. Rapp, ed.), NACE-6, pp 493-501 (1983)

12.   ROSNER, D. E., NAGARAJAN, R., GOKOGLU, S. A. and KORI, M., 'Maximum Effect of Vapor Phase Chemical Reactions on CVD-Rates and Deposition Onset Conditions in the Absence of Interfacial Kinetic Barriers', to be presented at the 10th Intl. Conf. on Chemica. Vapor Depo. 'tion (CVD-X), 172nd Meeting of the Electrochemical Society, October 18-23, 1987, Honolulu, Hawaii

13.   SCHAB, H. W. and GESSNER, F. R., 'Reduction of Oil-Ash corrosion by Use of Additives in Residual Fuels', Research and Development Report 070034C, NS-072-504 (April 1957), U.S. Naval Engineering Experiment Station

14.   Rathnamma,D.V. and D.W.Bonnell," Contaminated Fuel Combustion And Material Degradation Life Prediction Model", Proceedings Vol II, "High Temperature Alloys for Gas Turbines and Other Applications 1986" Reidel Publishing Co, Editors W. Betz, R.Brunetaud, D. Coutsouradis etc, pp 1105-1122.

15.   NAGARAJAN, R., Theory of Multicomponent Chemical Vapor Deposition (CVD) Boundary Layers and Their Coupled Deposits, Ph.D. Thesis, Dept. of Chemical Engineering, Yale University, May 1986

16.   RATHNAMMA, D. V. and R. NAGARAJAN, 'High Temperature Hot Corrosion Control by Fuel Additives (Contaminated Fuels)," in:Proc. 10th International Congress on Metallic Corrosion, 7-11 Nov 1987, Madras, India, Oxford and IBH Publishing, Vol. IV, pp. 3651-3664.

17.   STEWART, W. E., 'Convective Heat and Mass Transport in Three-Dimensional Systems with Small Diffusivities', Physicochemical Hydrodynamics, 1, 23-63 (1977)

18.   CUTLER, A. J. B., 'Molten Sulfates', in Molten Salt Techniques, Plenum Press, NY (1983)

19.   JANZ, G. J., ALLEN, C. B., BANSAL, N. P., MURPHY, R. M. and TOMKINS, R. P. T., 'Physical Properties Data Compilation Relevant to Energy Storage. II. Molten Salts: Data on Single- and Multi-Component Salt Systems', NSRDS-NBS, 61, Part II (1979)

20.   MOELWYN-HUGHES, E. A., Physical Chemistry, II Revised ed., Pergamon Press, NY (1964)

21.   ROSNER, D. E. and NAGARAJAN, R., 'Transport-Induced Shifts in Condensate Dewpoint and Composition in Multicomponent Systems with Chemical Reaction', Chem. Eng. Sci., 40, 177-186 (1985)

22.   ROSNER, D. E., Transport Processes in Chemically Reacting Flow Systems, Butterworth Publishers, Stoneham, MA (1986)

23.   GORDON, S. and McBRIDE, B. J., "Computer Program for Calculation of Complex Chemical Equilibrium Compositions, Rocket Performance, Incident and Reflected Shocks, and Chapman-Jouguet Detonations', NASA SP-273, Interim Revision, March 1976

24.   LUTHRA, K. L. and SPACIL, H. S., 'Impurity Deposits in Gas Turbines from Fuels Containing Sodium and Vanadium', J. Electrochem. Soc.: Solid State Sci. Technol., p 649, March 1982

25.   Cook, L.P, D.W.Bonnell, and D. Rathnamma, 'Corrosion and Corrosive Degradation of Ceramics', Ceramic Transactions, Vol 10, Editors: Richard E. Tressler. Michael McNallan. 1990, pp 251-276

26.   RATHNAMMA,D.V. AND R. NAGARAJAN," Hot Corrosion Life Prediction Model for Marine Gas Turbine Blades and Guide Vanes" Proceedings of the TRI-SERVICE CONFERENCE ON CORROSION" Editor: Milton Levy, Army Research Laboratory, Water Town, Massachusetts May 12-14,1992, pp271-285.

14

TABLE 1. **MOLTEN SALT DEPOSITS IN COMBUSTION TURBINES BURNING VANADIUM CONTAMINATED LIQUID FUEL**

EFFECT OF METALLIC ADDITIVES ON CONDENSED PHASE COMPOSITION

(ATOMIC RATIO OF ADDITIVE-TO-VANADIUM = 6:1)
SURFACE TEMPERATURE = 1600 F)

ADDITIVE	RELEVENT SOLUTION	SPECIES MOLE FRACTION			CONDENSATE FR.
		$Na_2SO_4(l)$	$Na_2V_2O_6(l)$	$V_2O_5(l)$	
NONE	$Na_2V_2O_6-V_2O_5$		0.265	0.293	1.36×10^{-06}
TITANIUM	$Na_2V_2O_6-V_2O_5$		0.28	0.73	1.30×10^{-06}
BARIUM	$Na_2SO_4-Na_2V_2O_6$	0.87	0.10		3.50×10^{-07}
STRONTIUM	$Na_2SO_4-Na_2V_2O_6$	0.91	0.054		3.50×10^{-07}
ZINC	$Na_2SO_4-Na_2V_2O_6$	0.028	0.0079		1.20×10^{-07}
SODIUM	$Na_2SO_4-Na_2V_2O_6$	0.83	0.16		8.10×10^{-06}
INDIUM	$Na_2SO_4-Na_2V_2O_6$	0.97			3.80×10^{-07}
NICKEL	$Na_2SO_4-Na_2V_2O_6$	0.49	0.46		3.65×10^{-07}
IRON	$Na_2SO_4-Na_2V_2O_6$	0.96	0.0049		3.40×10^{-07}
MANGANESE	$Na_2SO_4-Na_2V_2O_6$	0.67	0.30		3.55×10^{-07}
CADMIUM	$Na_2SO_4-Na_2V_2O_6$	0.97	0.0016		3.40×10^{-07}
CERIUM	$Na_2V_2O_6-V_2O_5$		0.35	0.64	1.00×10^{-07}
NEODYMIUM	$Na_2SO_4-Na_2V_2O_6$	0.78	0.18		3.50×10^{-07}
LANTHANUM	$Na_2SO_4-Na_2V_2O_6$	0.38	0.58		3.70×10^{-07}
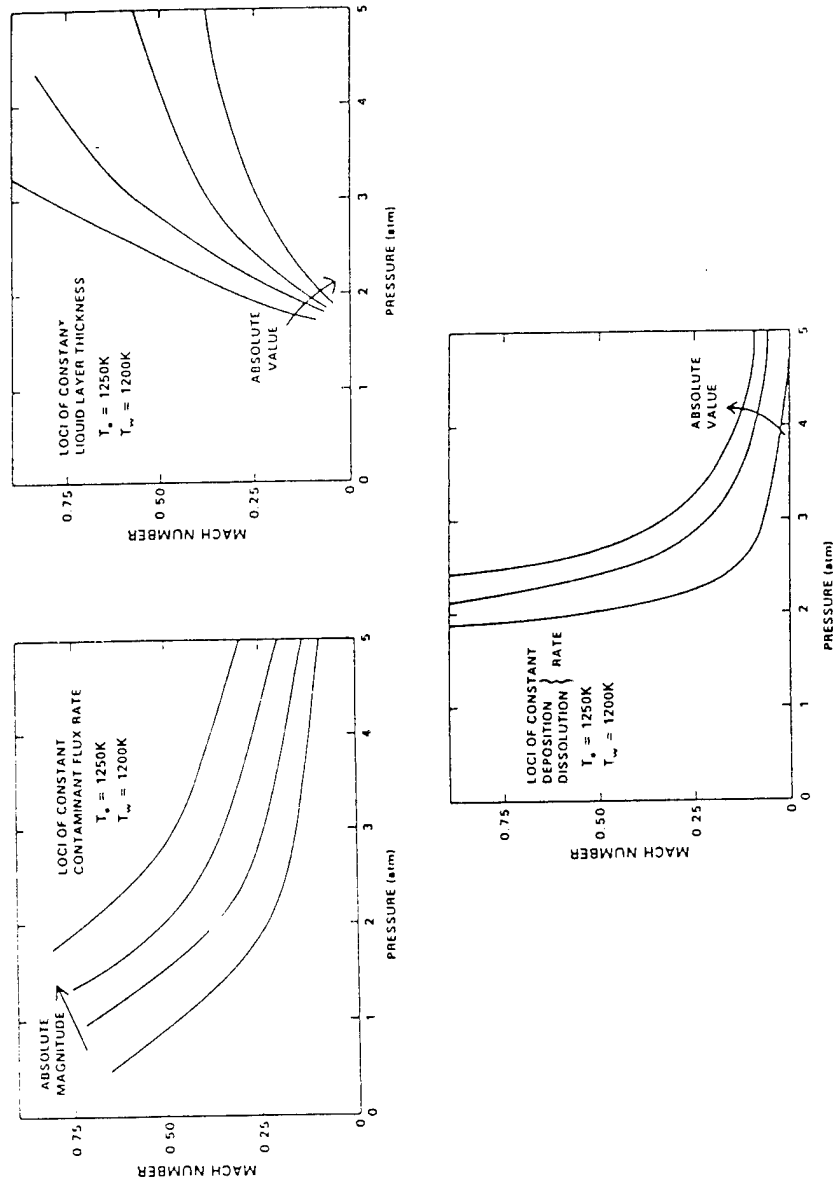
FIG 1. Simulation- charts for rig-design to reproduce
desired characteristics of the high-pressure turbine

CORROSION AND DEPOSITION EFFECTS OF OIL SOLUBLE ADDITIVES ON A HIGH TEMPERATURE ALLOY (AFTER SCHAB, 1957)
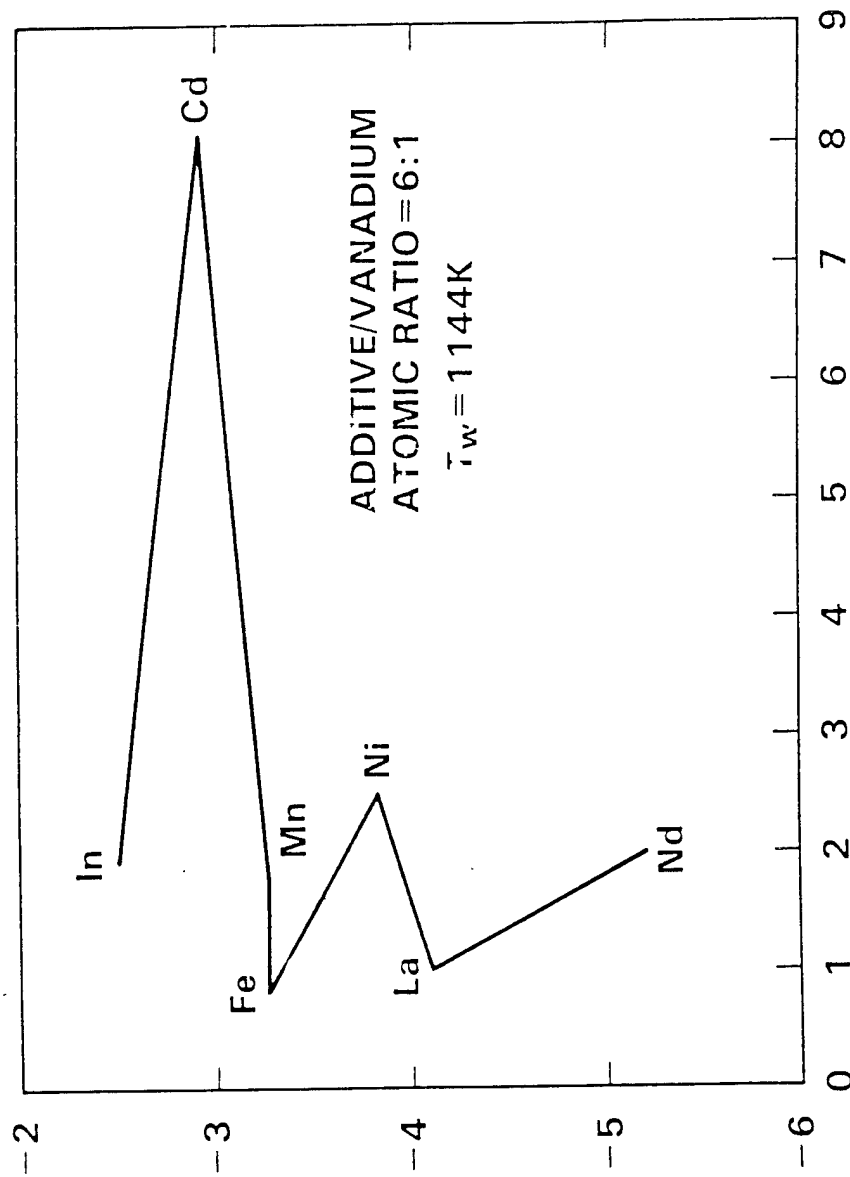
FIG 2.

17

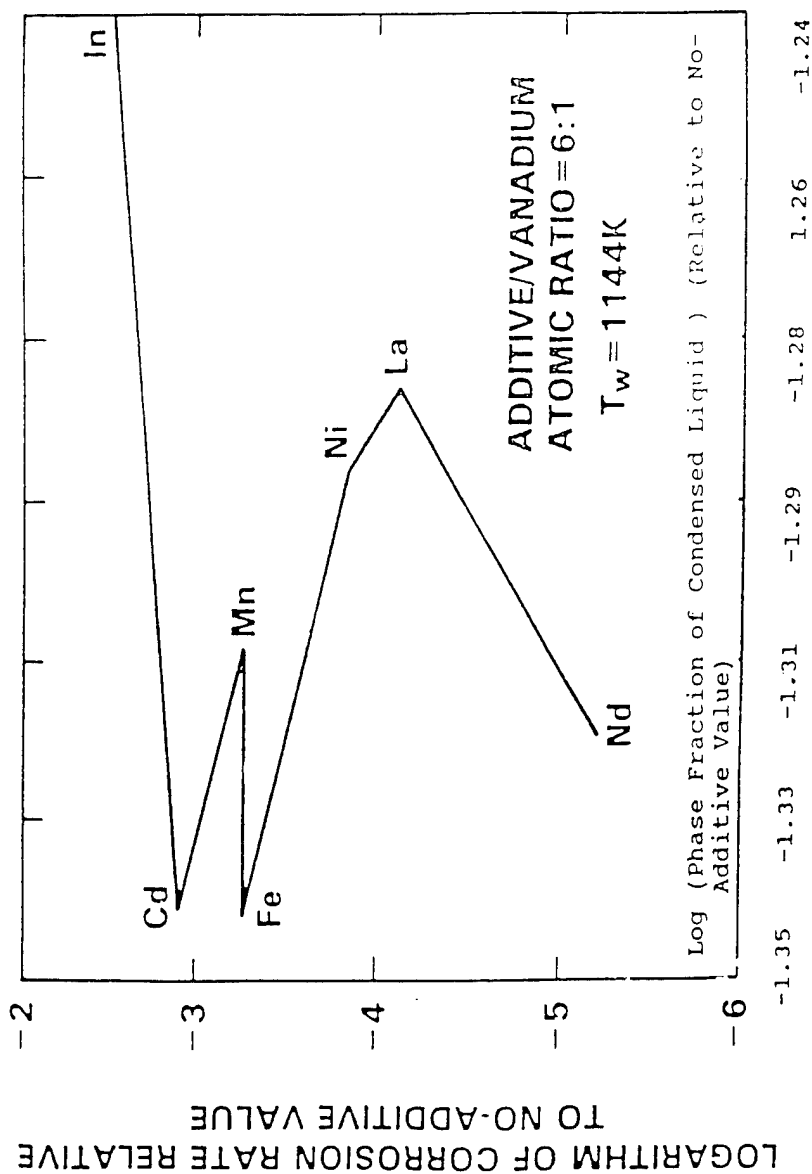FIG 3. Total weight (Solids + Liquid) of Deposit (relative to no-additive value) (data from the bar graph)

18

FIG 4. CORRELATION OF MEASURED CORROSION RATE DATA WITH CEC
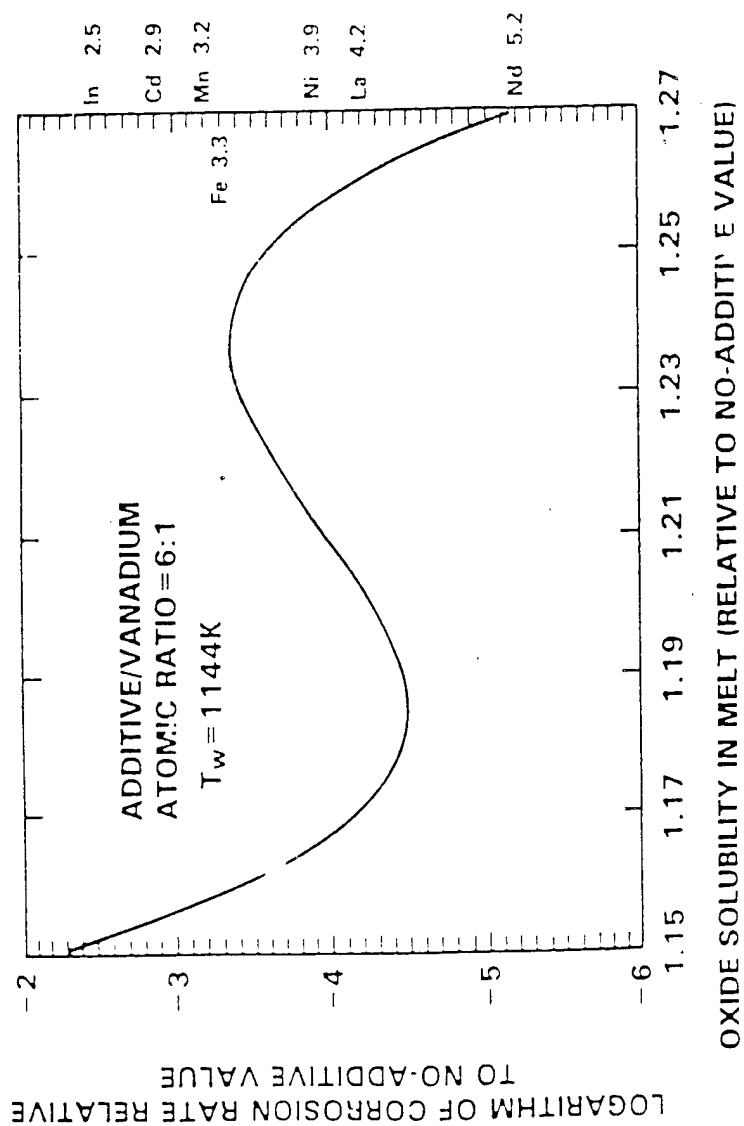PREDICTED LIQUID CONDENSATE MOLE FRACTIONS IN COMBUSTION
PRODUCT GASES

FIG 5. CORRELATION OF MEASURED CORROSION RATE DATA WITH COMPUTED
'IDEAL' SOLUBILITY OF OXIDE IN THE CONDENSED LIQUID

20

LOGARITHM OF CORROSION RATE RELATIVE TO NO-ADDITIVE VALUE

LOG (CONDENSED SOLUTION DEPOSITION RATE)
(RELATIVE TO NO-ADDITIVE VALUE)

ADDITIVE/VANADIUM
ATOMIC RATIO = 6:1
$T_w = 1144K$
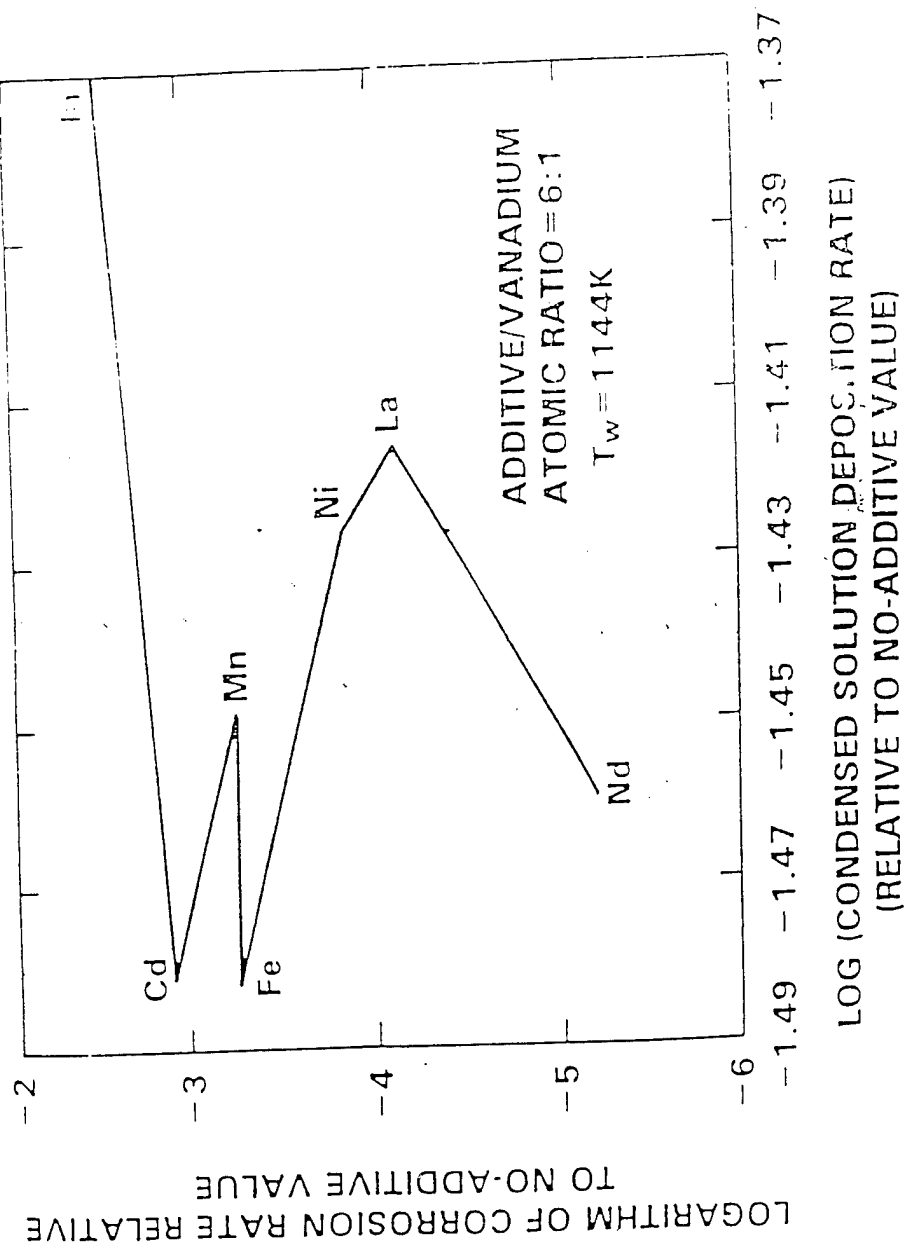
FIG 6   CORRELATION OF MEASURED CORROSION RATE DATA WITH COMPUTED
TOTAL DEPOSITION RATE OF LIQUID 'SOLVENT'-SOLUTION
(SAME FIG AS 5 WITH X-AXIS NUMBERS CHANGED)

21
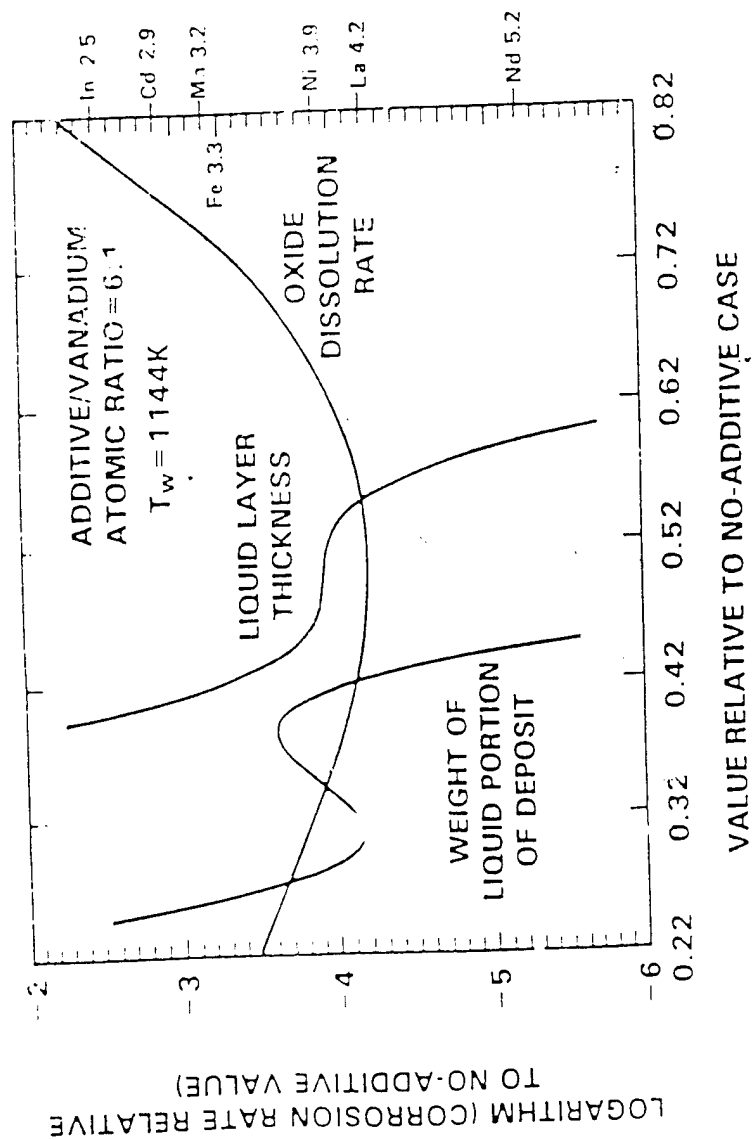
FIG 7.   CORRELATION OF MEASURED CORROSION RATE DATA WITH COMPUTED LIQUID LAYER WEIGHT AND THICKNESS AND OXIDE DISSOLUTION RATE

22

Detection and Thickness Characterization by X-Ray Backscatter of Second-Layer Corrosion in Aircraft Structures

Dr. L.R. Lawson, Mr. N.Kim and Prof. J.D. Achenbach*

Center for Quality Engineering and Failure Prevention
Northwestern University
Evanston, IL 60208-3020

SUMMARY

This paper briefly describes the Concept, the Equipment and the Preliminary Validation of an X-Ray Backscattering Technique to obtain quantitative thickness profiles of layered aircraft structures for the purpose of detecting and characterizing second-layer corrosion.

The features of the system may be summarized as follows

- Gives a cross-sectional view of aircraft sheet metal joints.
- Allows dimensional measurement and material identification of sub-surface layers.
- Only one-sided access needed. Not a transmission (shadow casting) technique.
- 1/1000 inch measurement accuracy.
- No evacuations. Does not interfere with hangar activity.
- Self-propelled. Scaffolding and stands are not needed.
- Data are digital files. Easily stored and transmitted via Internet.

INTRODUCTION

Until now, Compton backscatter imaging has had little commercial application to the detection of aircraft corrosion, even though its ability to image structures without requiring access to both sides is a valuable asset and in spite of the presence of commercially available equipment [1] . Until recently, the highest reported resolution in a Compton backscatter imaging system was only about 1.5 lp/mm [2] . This is not sufficient to resolve metal loss sufficiently for aircraft applications. The flux and noise considerations of Compton backscatter imaging have been reviewed elsewhere with reference to nondestructive testing [3] . Several designs for Compton backscatter imaging devices have been reported [1,2,4,5] .

Extensive technical details have been given elsewhere [6] .

23

WHAT IS X-RAY BACKSCATTER DEPTH PROFILOMETRY?

Compton x-ray backscatter depth profilometry , abbreviated X-Ray BDP, is a digital imaging technique for examining cross-sections of layered structures. It is based on the backscattering of x-ray photons toward a detector. The technique was developed specifically for the inspection of aircraft structures for corrosion as seen in the cover illustration. Unlike conventional radiographic techniques and CAT scanning, it is not a shadow-casting technique. The important difference is that X-Ray BDP gives a true *cross-sectional* view of the object being examined while in conventional (transmission) radiography, all information on structural features within the beam is superimposed in a single recording. The other major difference is that, unlike conventional radiography, X-Ray BDP does not require access to both sides of the object being examined. It can perform inspec ions of aircraft structures from the outside of the plane.

X-Ray BDP is designed to provide a highly accurate depth profile in locations of interest. It eliminates the costly down time needed for rivet removal required for direct measurement with calipers. It also eliminates the potential for fatigue crack initiation caused by bending the sheet metal in order to get the calipers in place or make a visual inspection. A point measurement technique such as X-Ray BDP is needed when there is an indication of corrosion by pillowing or some other broad-area inspection method such as eddy current scanning, ultrasonic scanning or possibly thermal wave imaging. These methods give a 2-D map of the near sub-surface region quickly, but they have not been able to generate cross-sectional views of much accuracy nor depth profiles. X-Ray BDP gives that additional information about thickness which is needed to make the decision of whether or not repairs are needed -- and how soon.

To collect backscatter data, the special depth-profiling camera shown in figure 1 was developed. The camera, which includes the x-ray tube, consists of a radiation d⌣ ector and a precision anisotropic collimation system for both the source and the detector. Four ap⌣ ⌣res define collimation, as shown in figure 1. The first two form the beam into a pencil with a narrow rectangular cross-section. The second two apertures select a limited-thickness region from which backscattered photons reach the detector. The selected backscattered beam falls upon a thallium-doped sodium iodide scintillation detector placed outside aperture 4. The intersection of the incident and backscattered beam paths forms a scattering zone. Sweeping this scattering zone through the structure to be examined allows visualization along the path of the electron density of the material, which for aluminum and lighter element⌣ is proportional to their mass density . The camera is mounted on a positioner which scans it in a direction perpendicular to the surface of the structure.
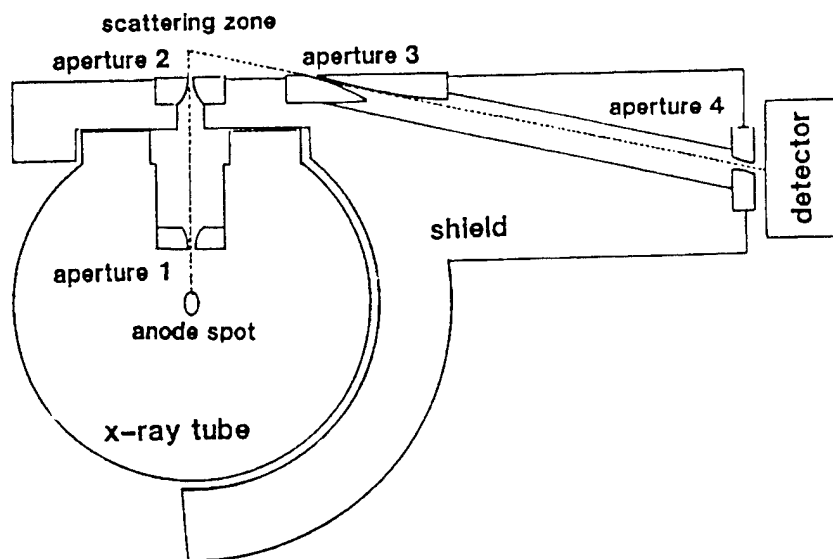
24

Fig. 1   Schematic representation of the backscatter camera

Like in other backscattering methods, the X-Ray BDP equipment could be used to generate 3-D images of entire volumes of material. Such an approach would, however, be very slow. In order to maximize the utility of backscatter data for aircraft inspection, X-Ray BDP reduces the image to one dimension. This makes the acquisition time on the order of 10 minutes per image--a practicable amount of time. The resulting image may be thought of as that of a core-drilled sample taken through the structure. The term "virtual core drill" has been coined to describe the X-Ray BDP machine for this reason. The design of the X-Ray 3DP apparatus takes advantage of this limited dimensionality to obtain higher flux for a given resolution than could be obtained with a conventionally-designed backscatter imaging system. The shape of the scattering zone is made anisotropic and the beam angles are correspondingly chosen to maximize the flux.

The resolution of the X-Ray BDP system has been chosen to measure the thickness of the layers of aircraft skin with an accuracy of ± 0.001" which is about that of a common grade of dial caliper. This is near to the best accuracy obtainable when measuring metal which has not been polished smooth. Manufacturing tolerances, and of course corrosion, both limit the smoothness of real surfaces. Furthermore, measurement errors typically add quadratically on the average. Thus if a micrometer having a ± 0.001 inch accuracy were used to measure a surface having 0.001" roughness, than the average measurement error would be ± 0.0014". This is not the best accuracy possible with the X-Ray BDP technique but is close to the best meaningful accuracy possible since surface roughness less than ± 0.001" is not typical for most surfaces on aging aircraft structures.
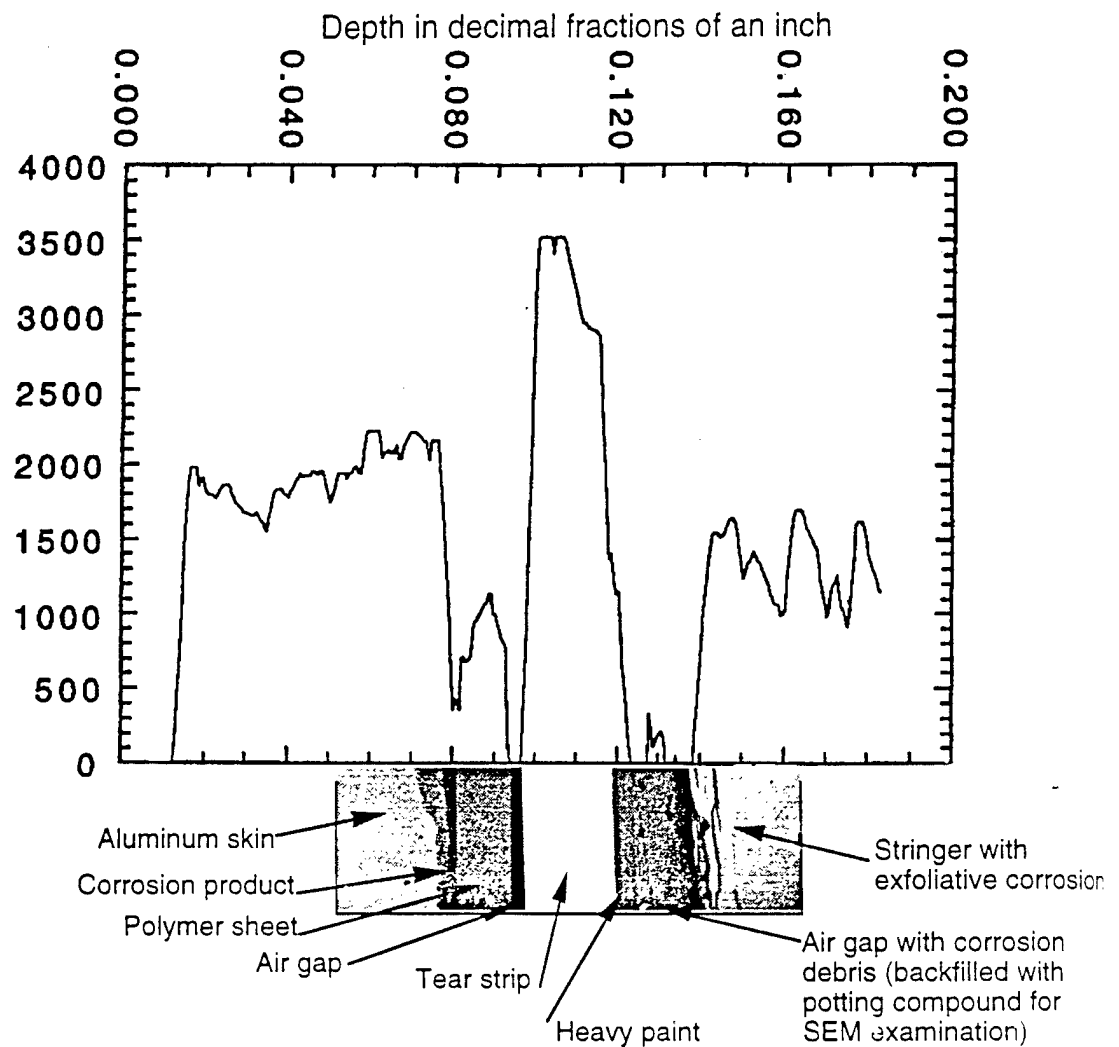
Depth in decimal fractions of an inch

Fig. 2 Comparison of an X-Ray BDP scan, above, with an electron micrograph, below, of a cross section of an aircraft sheet metal joint.

    X-Ray BDP reveals the details of layered aircraft structures. Figure 2 shows a comparison of an X-Ray BDP scan with an electron micrograph of a core sample drilled from the same location on a fuselage. The vertical axis on the scan represents the relative density of the material. The horizontal axis represents the depth into the fuselage measured from a point slightly above the surface at which the scan began. The electron micrograph displays the region between the outer skin and a stringer. In the scan, the outer layer, of aluminum, appears as a boxcar starting near 0.01". There follows a low-density region a couple thousandths of an inch in thick followed by a piece of plastic sheet, a faying strip, nearly 0.012" thick. Following that strip, there is an air gap. Beyond that gap, is a

stainless steel tear strip. The tear strip has a higher density than the aluminum. The back side of the tear strip is painted. Beyond the tear strip is a large air gap containing corrosion debris. Then follows the the stringer. The paint on the back side of the tear strip is discernible. The stringer appears to be less dense than the skin, which is the result of iron in the tear strip exerting a shielding effect on layers beneath it. The presence of the heavy element, iron, in the tear strip can be deduced from the tilting down to the right of the top of the tear strip's boxcar while those of aluminum are flat.

Indications in a scan of unexpected low-density material, air gaps and thinning of metal are the hallmarks of corrosion in an aircraft structure.The presence of loose low density material signals active or untreated corrosion. Air gaps alone, unless greater than a few mils in width, do not by themselves indicate corrosion. Within the present field experience with X-Ray BDP, air gaps seem to be present in all joints in older aircraft. On one hand this is a benefit since it makes possible accurate determination of metal thicknesses while using larger data collection step sizes than would be otherwise allowable. But, it is the presence of these gaps which give rise to water trapping and corrosion in the first place. Corrosion products, when compacted, often appear as material having about half the density of their parent aluminum. Loose corrosion products often have still lower densities.

The corrosion process itself appears to determine the relatively low density of corrosion products as seen in X-Ray BDP. Water typically collects in small gaps between metal layers. Salts or other ionizable species from waste products, air pollution, ocean spray etc. find their way into the water. Chlorides appear to be especially detrimental. Sometimes ions of more noble metals such as copper also get into the joint . These can set up local electric currents which dissolve the aluminum much as the anode of a battery. More often the water and the thinness of the gap prevent air from entering uniformly. The parts of the gap that are deep inside become anodic due to the relative lack of oxygen and this sets of electric currents which dissolve the aluminum in these recesses. This process is called crevice corrosion. In all cases, ions must move through the corrosion product layer to support the electric current. This means that all corrosion products must be porous in order to grow. Their pores are the primary reason that corrosion products are less dense than aluminum itself. Figure 3 shows an electron micrograph of undisturbed corrosion product on the surface of a second-layer of skin. The relative volume of pores is 40%. The pores are the channels for the corrosion current to flow. Without pores, the corrosion product would be protective films since oxides and hydroxides are, by nature, insulators and ions cannot diffuse through them directly at temperatures below about 1000°C.
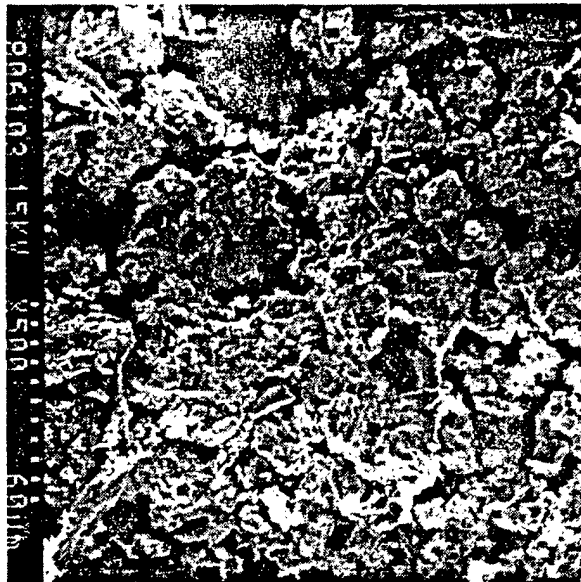
Fig. 3 Corrosion product on the surface of a second-layer of fuselage skin

HOW DO YOU USE X-RAY BDP?

The cover illustration shows X-Ray BDP being used to inspect a station along a lap splice on the Boeing 737 located at the FAA/AANC facility in Albuquerque, NM. The X-Ray BDP unit moves around under its own battery power. The unit is positioned at the point where the scan is to take place, and the scan head is guided to the exact location by an operator (typically on a ladder). The operator controls the boom and can pivot the scan head. When the scan head is in place, four feet rest against the planes surface. Then by operating the boom, the scan head is pressed against the plane. Friction of the feet against the surface holds the scan head in place. The boom itself is a giant spring which is constructed so as to have compliance in the axial as well as lateral directions. The boom supports the scan head and simultaneously applies pressure normal to the bottom surface of the scan head's feet in whatever position the head may be placed. The cover shows the scan head being pressed against the side of the plane. Figure 4 shows the scan head lifted into position for inspection of the belly section of an aircraft. The scan head when in use is thus aligned with the surface of the plane but is sufficiently independent of the motorized carriage, which transports it.

Once in place, the scan head is precisely re-aligned by computer-controlled stepper motors using position sensors which contact the plane; and, then the scan begins. Figure 5 shows the scan head. One of the motors is visible in the lower foreground; two of the four feet are seen at the
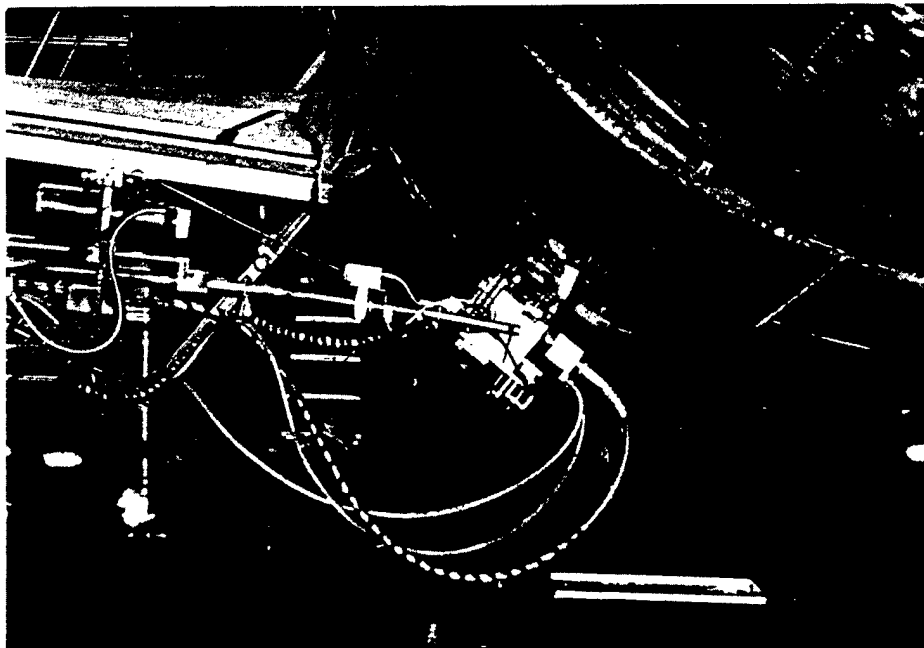
Fig. 4 X-Ray BDP Scan in place underneath an aircraft for scanning the belly section.
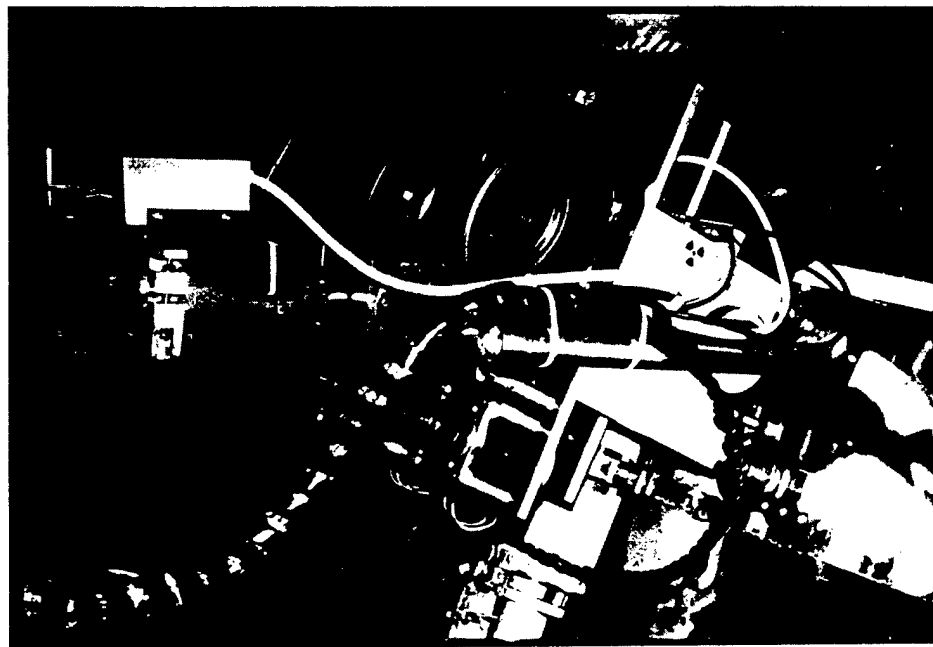

Fig. 5 Scan head. One of the stepper motors and two of the feet are visible.

right. The computer performs the scan, advancing the motors and stopping at intervals to collect data. These intervals are steps of usually 0.001" or 0.002". Because an edge appears as a slope in the unprocessed data, the edge can be precisely located so long as two data points are taken along the slope. Thus, for example, in principle, a 0.002" step will precisely locate an edge(within say 0.0001") provided that there is a gap of 0.004 or more inches between that edge and the next one. Of course, noise degrades this precision and the main source of noise is the statistical nature of photon counting. As a rule of thumb, 1000 counts are needed to locate the edge in the example to within 0.001". Increasing the number of counts increases the precision. While the scan is being made, the x-ray tube is operated typically at 150 KV and 15 mA. This means that, within the tube, a great deal of radiation is being generated, but very little of this radiation escapes. Only a
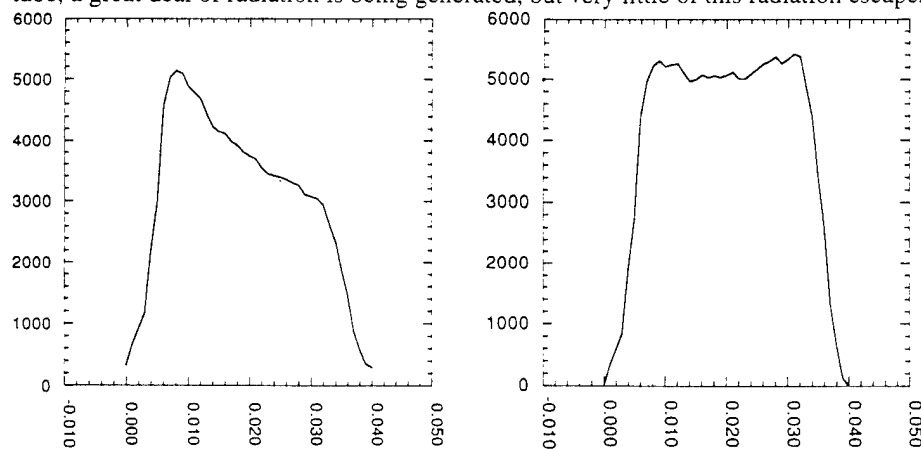
Figs. 6a,b Raw(a) and reconstructed(b) data for a scan through a single layer
The x-axis is depth in decimal inches, the y-axis is relative density.
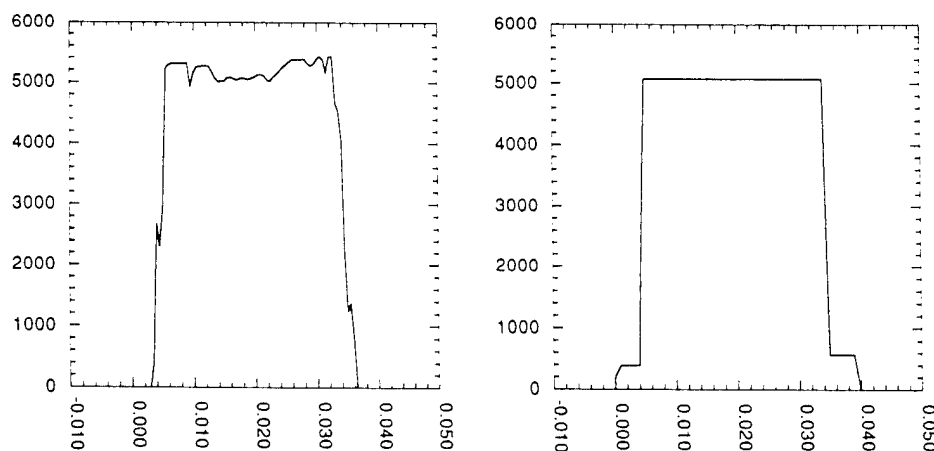
Figs. 6c,d Deconvolved(c) and blocked(d) data.

30

very tiny beam is actually used. Heavy shielding near the x-ray tube is needed to confine the beam. Consequently, very little radiation escapes into the environment. During scanning, the radiation level is low enough that, by the standards of most States, workers who are not designated radiation workers may safely approach within as little as three feet from the operating x-ray tube. Greater than ten feet from the operating tube, the radiation level is extremely low. Mechanics may thus work on the outside of the plane in the vicinity of X-Ray BDP scanning. Because some of the beam becomes trapped inside, working inside the plane during scanning might be inadvisable. But the worst dose of radiation measured on the inside of a plane, directly on the other side of a fuselage skin at the point of irradiation, still amounted to only the equivalent of one chest x-ray per hour. During the scanning, the computer rechecks alignment and realigns the scan head as needed. If the count rate drops to too low a value, the computer interrupts the scan and queries the operator for instructions.

When the scan is completed, the computer displays the result as a graph similar to that in figure 2. Several processing steps are involved. These are illustrated in figures 6a-d. Figure 6a shows the raw data for a scan through a single piece of metal. The effect of reconstruction is shown in figure 6b. Reconstruction mathematically removes the shadows of upper layers on lower ones. In the case of a single layer it converts a boxcar with an exponential top, figure 6a, into one with a flat top, figure 6b. The next step removes the blurring effect of the aperture upon edges. This blurring effect gives sloping sides to the boxcars in figures 6a and 6b. Figure 6c shows the sides squared through deconvolution. A still more idealized form is obtained by further processing called "boxing" or "blocking". Blocking applies a slope threshold method of edge finding to the deconvolved data. A table of layer thicknesses is an important byproduct of the process. Unfortunately, this type of processing slightly degrades the accuracy of the measurement. A less-speedy approach based on using the deconvolved or blocked image as a guide to finding the actual edges in the raw data gives superior results.

EXAMPLES OF X-RAY BDP

The two examples which follow were taken from scans made at the FAA/AANC Validation Center, as part of the preliminary validation process of X-Ray BDP.

Figure 7 shows a scan of the Boeing 737 at the FAA/AANC facility. The scan is taken through a lap joint along the middle row of rivets. The scan has been processed through the deconvolution step shown in figure 6c. Large air gaps and loose material suggest the presence of corrosion. The front layer of skin measured 0.0375" using the deconvolved plot. The expected

31

accuracy under these circumstances is an average absolute error of 0.0015". Better accuracy could have been obtained by fitting the raw data, as mentioned above, but this is not yet routine.
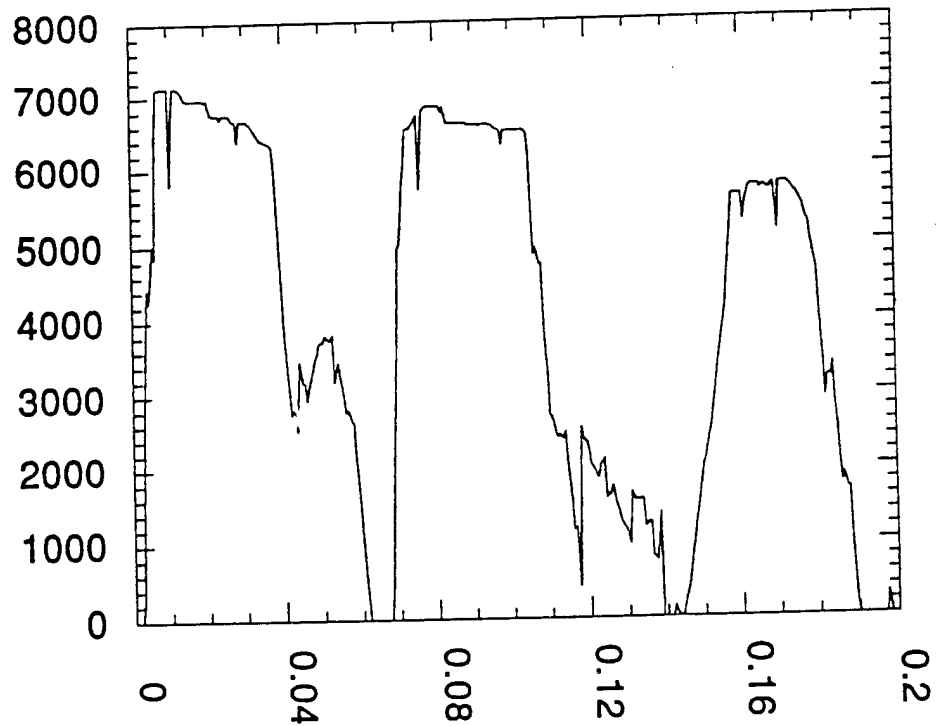

Fig. 7 Scan through a lap joint. Three metal layers are shown.

In what follows, the thicknesses will be quoted to the apparent accuracy on the scan, three or four decimal places, in order to avoid inviting cumulative rounding errors, since the accuracy of two layer thicknesses added together is still the same as that for each layer. Beneath the front layer was a f /ing strip of possibly scrim cloth and sealant. It resembles the layer of polymer seen in figure 2. The scan suggests that this layer has become detached from the front layer leaving a 0.001" gap. The low-density faying layer measured 0.0175". Below the faying layer was another air gap, 0.0097" wide. The second layer of skin, which begins below this gap, measured 0.0403". Its rear surface looks rough as indicated by the sloping of its front surface being asymmetrical to that of its back surface. It may also have been painted with primer. A small-step long-count-time scan of just the interface could be used to resolve this issue were it important. Beneath this layer of skin are the remains of another faying strip, probably reduced to an aggregate of sealant and corrosion product. It measured 0.0212". Its unusually-low density and looseness are strong indicators of corrosion. Beneath this is yet another air gap 0.0138" wide. The last layer is the

stringer itself. It measures only 0.0355". Micrometer examination within the plane showed that the stringer was indeed about this thickness.

Figure 8 shows a scan of a boron epoxy patch applied to a cold-bonded skin on the same plane. Although boron has a low atomic number, the density appears as if it were higher than that of aluminum. This is partially the result of the very low x-ray absorption coefficient of this material. The patch measured 0.0245" thick and appears to be composed of two layers of boron fiber separated by a layer of epoxy. The outer layer measured 0.013" while the second layer of patch measured 0.0105". Between the two layers was a layer of epoxy, about one mil thick. Beneath the patch at the point where the scan was made there appears to be a disbond with a gap 0.0035" wide. There also appears to be some warpage since the planes of the aluminum and the patch are not parallel at the interface. Underneath the patch is a bonded skin composed of two layers of aluminum. The first layer measured 0.038" thick while the second measured 0.0343" thick. The resin bond between the two layers measured about 0.003".
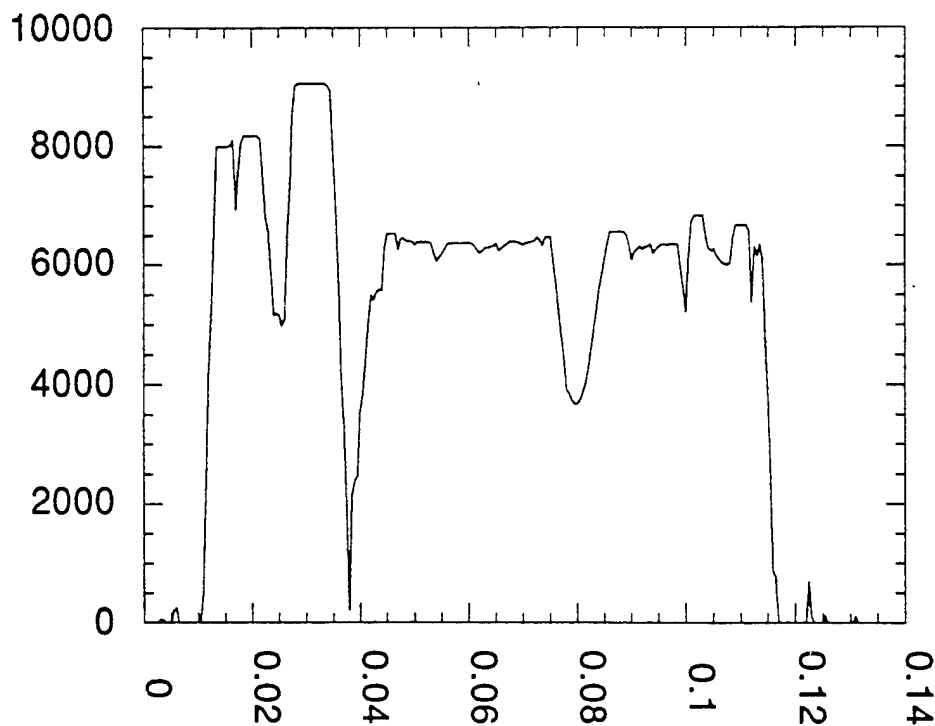

Fig. 8 Scan through a boron-epoxy patch applied to a cold-bonded skin.

33

Mobile X-Ray BDP unit in place for a scan of a lap joint of a B737

ACKNOWLEDGMENT

REFERENCES

1. J. Kosanetzky et al., "Compton Back-Scatter Tomography of Low Atomic Number Materials with the Com-Scan System," Phillips Forschungslaboratorium, Hamburg (no date).

2. J. Smith, "Backscatter Imaging Tomography BIT (T.M.), presented "Advanced Development Computed Tomography Program, Industry Demonstrations and CT Workshop," Wright Laboratory/Hill Air Logistic Center, Salt Lake City, UT, May 5-7, 1992.

3. L. Lawson, in Review of Progress in Quantitative Nondestructive Evaluation (D.O. Thompson and D.E. Chimenti, Eds.), Vol. 11A, pp. 315-322, Plenum, New York, 1992.

4. J.A. Stokes, K.R. Alvar, R.L. Corey, D.G. Costello, J. John, S. Kocimski, N.A. Lurie, D.D. Thayer, A.P. Trippe, and J.C. Young, Nucl. Instrum. Methods 193, 261-267 (1982).

5. H. Strecker, Mater. Eval. 40, 1050-1056 (1982).

6. L. Lawson, Journal of X-Ray Science and Technology 4, pp. 18-36, 1993.

34